NANO LETTERS

2009
Vol. 9, No. 4
1451-1456

Ultrastable Atomic Force Microscopy: Atomic-Scale Stability and Registration in Ambient Conditions

Gavin M. King,[†] Ashley R. Carter,[†,‡] Allison B. Churnside,[†,‡] Louisa S. Eberle,[†,§] and Thomas T. Perkins*[,†,||]

JILA, National Institute of Standards and Technology, and University of Colorado, Boulder, Colorado 80309, Department of Physics, Department of Molecular, Cellular, and Developmental Biology, University of Colorado, Boulder, Colorado 80309, and Denver School of Science and Technology, Denver, Colorado 80238

Received November 1, 2008; Revised Manuscript Received January 27, 2009

ABSTRACT

Instrumental drift in atomic force microscopy (AFM) remains a critical, largely unaddressed issue that limits tip−sample stability, registration, and the signal-to-noise ratio during imaging. By scattering a laser off the apex of a commercial AFM tip, we locally measured and thereby actively controlled its three-dimensional position above a sample surface to <40 pm ($\Delta f = 0.01-10$ Hz) in air at room temperature. With this enhanced stability, we overcame the traditional need to scan rapidly while imaging and achieved a 5-fold increase in the image signal-to-noise ratio. Finally, we demonstrated atomic-scale (∼100 pm) tip−sample stability and registration over tens of minutes with a series of AFM images on transparent substrates. The stabilization technique requires low laser power (<1 mW), imparts a minimal perturbation upon the cantilever, and is independent of the tip−sample interaction. This work extends atomic-scale tip−sample control, previously restricted to cryogenic temperatures and ultrahigh vacuum, to a wide range of perturbative operating environments.

Atomic force microscopy (AFM) is a crucial tool in diverse fields[1−3] and is most commonly applied in ambient conditions (i.e., in air at room temperature).[1] Historically, the AFM community has focused on developing sharper tips and higher-sensitivity force-detection schemes for improved microscope performance.[4−6] Yet, imaging and other AFM applications are limited by mechanical drift between the probe tip and the sample. Drift limits both tip−sample stability and registration. This stability is the capacity to hold the tip over a precise sample location. Tip−sample registration is the ability to return the tip to a particular feature in an image. While atomic-resolution imaging has been achieved at room temperature in both air[7] and liquid,[8] atomic-scale (∼100 pm) stability and registration have not. Precise three-dimensional (3D) control of the tip, the sample, and their relative position is needed to fully exploit AFM across a broad array of fields. For example, atomic-scale registration and stability would enable returning an AFM tip to a specific domain of a protein and then monitoring the protein's dynamics by "hovering" the tip over this domain for extended periods. Such an experiment, similar to the pioneering report of enzymatic activity measured via AFM,[9] would have the added assurance of long-term tip−sample stability.

There exist a handful of drift-compensation methods that exhibit varying degrees of success and usability. Tracking techniques[10−12] can yield atomic precision in ultrahigh vacuum, but they forfeit scanning or assume unvarying drift rates. Imaging-based techniques[13] can reduce drift rates to ∼500 pm/min in ambient conditions[14] but require predictions of future drift or compensate for drift only once per image. External optical techniques, applied in one[15,16] or more dimensions,[17−19] have not achieved atomic-scale tip−sample stability or image registration (<10 nm overlay precision)[19] in ambient conditions.

A local, high-bandwidth measurement of both the tip and sample position could form the foundation for a robust stabilization technique. Ideally, such a technique would be compatible with commercial tips. Local detection measures drift unseen by stage sensors, typically capacitors positioned several centimeters from the AFM tip. High bandwidth accommodates drift rates that fluctuate significantly during image acquisition (Supporting Information, Figure S1). Independent measurement of both the tip and sample places

* To whom correspondence should be addressed. E-mail: tperkins@jila.colorado.edu.
[†] JILA, National Institute of Standards and Technology and University of Colorado.
[‡] Department of Physics, University of Colorado.
[§] Denver School of Science and Technology.
[||] Department of Molecular, Cellular, and Developmental Biology, University of Colorado.

10.1021/nl803298q CCC: $40.75
Published on Web 03/12/2009

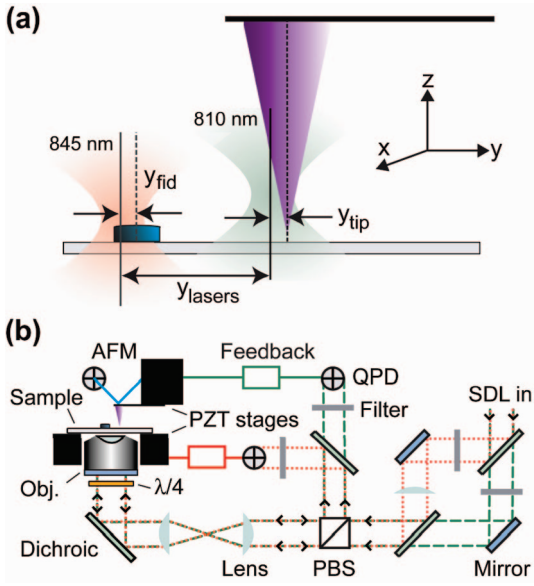

Figure 1. Schematic of the experimental layout. (a) Detailed view of the tip and sample shows focused lasers scattering off an AFM tip and a fiducial mark (silicon disk) on the sample. Back-scattered signals were collected and used to deduce the position of the tip and the sample relative to each laser beam. (b) Two stabilized diode lasers (SDL) at different wavelengths [λ = 810 nm (green), λ = 845 nm (red)] were sent into the microscope and focused by a high numerical-aperture objective (Obj). Back-scattered light was separated from the incoming light by an optical isolator formed by a polarizing beam splitter (PBS) and a quarter-wave plate (λ/4). At different wavelengths, the signals were separated by dichroic mirrors and detected by independent QPDs. A third laser [λ = 785 nm (blue)] was reflected off the backside of the cantilever for force control during AFM imaging. Tip and sample control were achieved via feedback loops to two PZT stages. Blue-shaded components are in optically conjugate planes. The long axis of the cantilever was along the *y*-axis.

no restriction on tip activities. Compatibility with commercial tips enables broad applicability.

In optical-trapping applications, laser-based detection of micron-sized beads using forward-scattered light provides high-bandwidth (>1 kHz) detection coupled with picometer-scale localization precision.[20] For AFM applications, we hypothesized that laser light scattered off the apex of the AFM tip (not its back side) could be used to locally measure the tip's position (Figure 1). We used back-scattered detection (BSD) because BSD uses a single lens to focus and collect the light, making it geometrically compatible with AFM. In contrast to classic interferometric detection that provides for single-axis measurement, BSD uses a single laser to measure position with atomic-scale sensitivity in 3D.[21] With such 3D detection, a pair of lasers creates a local, differential reference frame that enables an ultrastable AFM. The stability of the reference frame arises from the excellent differential pointing stability between the lasers (e.g., Figure 1a, δy_{lasers} = 20 pm).[21] Using this local reference frame on transparent substrates, we controlled the position of a commercial AFM tip in 3D with high precision (<40 pm, Δf = 0.01−10 Hz). Further, we increased the signal-to-noise ratio (*S*/*N*) of AFM images 5-fold via real-time averaging provided by stabilized slow scanning. Finally, we achieved atomic-scale tip−sample stability and registration in air at room temperature over tens of minutes.

For independent measurement and control of both the sample and the tip (six axes), we used a custom-built AFM mounted on an inverted optical microscope (Figure 1b). We measured position with a pair of focused detection lasers (λ = 810, 845 nm) that scattered separately off the tip and a fiducial mark (Si disk: radius ~ 300 nm, height ~ 60 nm) patterned onto a glass coverslip.[21] The resulting back-scattered signals were detected by a pair of quadrant photodiodes (QPD, YAG 444−4A, PerkinElmer Optoelectronics). Commercial silicon and silicon-nitride tips were used [CSC38/noAl (k = 0.08 N/m), MikroMash; DNP-S (k = 0.06 N/m), Veeco, respectively]. To establish excellent differential stability, the two BSD lasers were colaunched from a single fiber and actively stabilized.[22] These lasers were independently translated in the imaging plane by mirrors conjugate to the back aperture of the objective lens (PlanAPO-100X-IR, NA = 1.4; Nikon). The combination of a polarizing beam splitter and a quarter-wave plate formed an optical isolator for efficient collection of the back-scattered light.[21] The lateral position of both the tip and sample was deduced by the normalized lateral differences in optical power on the QPDs. The vertical position was deduced from the sum of the power falling on all QPD quadrants.[21] The vertical cantilever deflection, and hence the tip−sample force, was detected via a standard optical lever arm (Figure 1b, blue, λ = 785 nm).[23] The six axes of motion (i.e., x, y, z on both piezoelectric (PZT) stages, P363.3CD and P733.3DD, Physik Instrumente) were calibrated and controlled with custom software (LABView 8.5, National Instruments) along with a field-programmable gate array card (PCI-7833R, National Instruments). In this scheme, we achieved high bandwidth (500 Hz) control of both tip and sample.

Before imaging, we needed to establish that BSD could localize an AFM tip, a highly asymmetric object in comparison to beads and thin silicon disks. Ideally, such a signal would be sensitive to atomic-scale motion in 3D with low cross-talk between axes. To demonstrate these signals, we first positioned a silicon tip 300 nm above a glass surface in air and then sequentially translated it through the 810 nm laser focus along each axis, yielding a voltage-versus-distance curve, for example, $V^{QPD}(x_{tip})$ (Figure 2). The QPD signal during x-axis motion (Figure 2a, solid red line) monotonically decreased and was approximately linear, whereas the off-axis traces (Figure 2a, dashed blue and green lines) were relatively flat (<8% cross-talk over a 50 nm range). A 2-fold increase in the laser power used for BSD (from 400 to 800 μW at the tip) did not alter the shape or magnitude of the BSD signals but did introduce a slight z offset (<1 nm) of the tip. Analogous records were obtained for tip motion along the y and z axes (Figure 2b,c). Such BSD signals formed the basis for subsequent tip voltage-to-position calibration (see Supporting Information). With active reduction in laser noise and electronic amplification,[22] the resulting sensitivities (>6 mV/nm) were sufficient to detect picometer-scale motion.

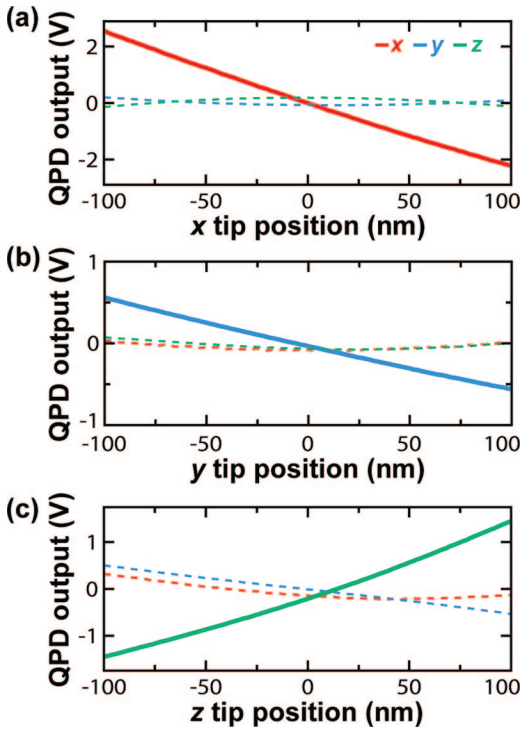

Figure 2. AFM tip detection in three dimensions. (a−c) Records of the QPD output vs tip position are shown for x (red), y (blue), and z (green) on the moving axis (solid lines) and the stationary axes (dashed lines) from light scattered off a commercial silicon tip. Traces offset vertically for clarity.

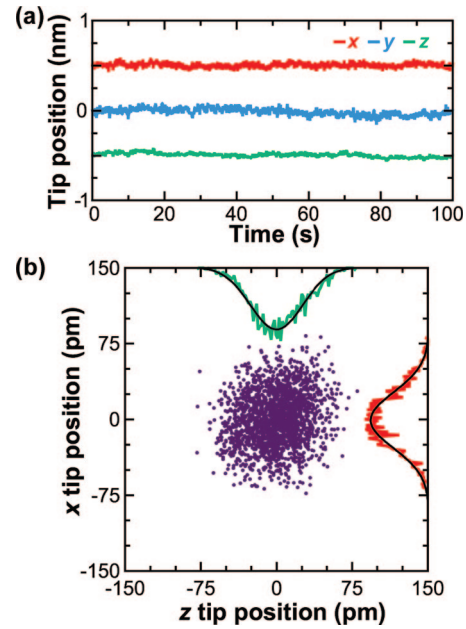

Figure 3. Picometer-scale AFM tip control in 3D at ambient conditions. (a) Tip position records vs time were low-pass filtered to 10 Hz and offset vertically for clarity [x (red), y (blue), z (green)]. Positions were determined by an "out-of-loop" monitor laser while the tip was actively stabilized with the other laser. (b) A scatter plot of the tip position in the $x-z$ plane from the 100 s record in panel a. Histograms of the data projected onto the x and z axes were well fit by Gaussians with standard deviations of 28 and 26 pm, respectively.

BSD-based tip detection is robust to small optical changes in the local detection volume and compatible with several different environments and substrates. In the current implementation, we used transparent substrates in air, but we have also achieved tip-based BSD signals in liquid and through thin metal films on glass (Supporting Information, Figure S2). Since the detection beams pass through the sample, degradation of the signal due to scattering from the sample could lead to erroneous tip positioning. To quantify this effect, we scanned 5 nm gold nanospheres through the tip-stabilization laser beam. At the gain amplifications used for measuring tip motion, we found no signal. However, larger gold beads (diameter = 15 and 40 nm) produced a small perturbation on the AFM tip signal (2 and 7%, respectively). In principle, the optical-scattering signal of the tip detection laser due to the sample could be recorded at each pixel with the tip retracted and then subtracted from the total tip signal during imaging. The high degree of sample stability and registration ensure that no significant drift will occur and that such background subtraction would remain valid for long durations.

We next used these BSD signals to measure and actively control the position of an AFM tip in 3D above the sample surface (Figure 3). For this demonstration, both detection lasers were focused onto a silicon tip (i.e., Figure 1a, $y_{\text{lasers}} = 0$) positioned 300 nm above the glass surface. We employed the 810 nm signal for feedback and the 845 nm signal as an independent "out-of-loop" monitor.[21] Stabilities, determined from this out-of-loop monitor, were 26, 39, and 25 pm in x, y, and z, respectively (rms, $\Delta f = 0.01-10$ Hz). Thus, we demonstrated simultaneous lateral and vertical tip control at picometer length scales (Figure 3b). Histograms of this data provided a complementary analysis and were well fit by Gaussians, with standard deviations of 28 and 26 pm in x and z, respectively. These reported stabilities represent a metric for the ultimate positional control between tip and sample that can be achieved with our current apparatus and include the uncertainty due to 3D pointing noise between the detection lasers. Moreover, this direct measurement of tip position is independent of the traditional observable in AFM, cantilever deflection (Figure 1b, blue). Thus, BSD provides a complimentary, local measurement of tip position that is independent of the tip−sample force.

When imaging, precise tip−sample control can be exploited to increase *S*/*N* in real time by scanning slower to average the cantilever response. AFM cantilevers are subject to stochastic thermal excitation in addition to other noise sources that often couple into cantilever motion (e.g., acoustic, mechanical). Thermal motion, which has a zero mean, can be averaged at the expense of temporal resolution. In general, when studying slowly varying or static samples, it is preferable to average data for a long time with respect to the response time of the cantilever ($\sim$100 μs) and the characteristic time of other noise sources. However, in practice, most AFM images are acquired quickly, often to avoid drift.

The prospects for real-time *S*/*N* enhancement are predicated on effective averaging of cantilever response. We demonstrated this enhancement by acquiring cantilever response with the tip engaged at a single stabilized pixel

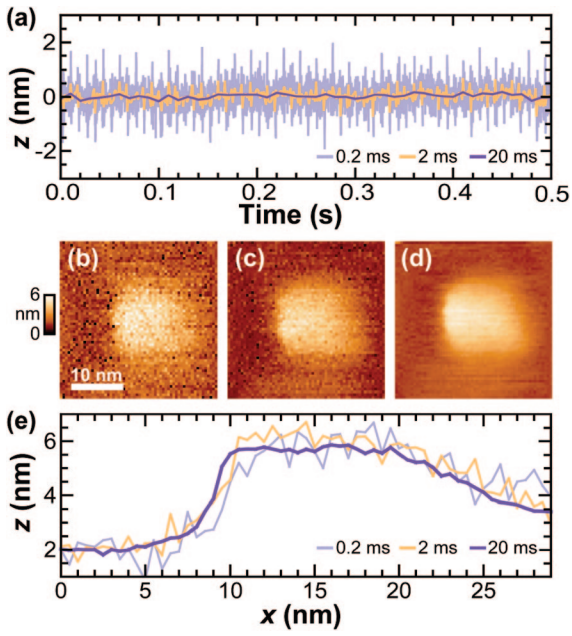

Figure 4. Improved signal-to-noise ratio in an image. (a) Time record of the cantilever-imaging signal when the tip was engaged on the surface and held stable at a single pixel. Analysis of these records showed standard deviations of 0.47, 0.24, and 0.09 nm when low-pass filtered to 5 kHz (light purple), 500 Hz (orange), and 50 Hz (dark purple), respectively. (b−d) Sequential images of a 5 nm gold nanosphere taken with increased averaging. Specifically, the averaging times per pixel were 0.2, 2, and 20 ms for panels b−d, respectively. (e) Line scans through the center region of images [b (light purple), c (orange), and d (dark purple)].

(Figure 4a). To do so, we stabilized all six axes of the stage and the tip. The three axes of the sample and the lateral position of the tip were stabilized using BSD signals. The vertical position of the tip was controlled to maintain a constant tip−sample force of ≈200 pN. We observed a 5-fold reduction in the standard deviation of the cantilever imaging signal from 0.47 to 0.09 nm for data smoothed to 5 kHz and 50 Hz, respectively (Figure 4a, see Supporting Information). Ideally, averaging white Gaussian noise over two decades in frequency should result in a 10-fold reduction in noise. Thus, we achieved a substantial (5-fold), but not ideal, increase in *S/N*.

Next, we demonstrated improved imaging by stabilized slow scanning (see Supporting Information for details and Figure S3). Specifically, we acquired three 30 × 30 nm^2 images of a single 5 nm Au nanosphere at increasing averaging times per pixel (0.2, 2, and 20 ms for Figure 4b,c,d, respectively) in contact mode ($F \approx 200$ pN). Improvement in image quality is visually apparent. Quantitatively, line scans through the center of each image (Figure 4e) also revealed a 5-fold reduction in the rms surface roughness over the center of the nanosphere. Thus, the successful reduction in cantilever noise at a single pixel was recapitulated during imaging. We note that for many applications, real-time averaging is superior to post processing of the images; it does not require assumptions of sample periodicity, symmetry, or image-to-image registration.

Finally, we designed an experiment to directly demonstrate atomic-scale tip−sample stability and registration. It is this registration and stability, not resolution, that is the unique feature of the instrument. Resolution, the ability to differentiate two neighboring objects, has been reported at the atomic scale in ambient conditions;[7] however, such resolution is not required to demonstrate atomic-scale stability and registration. Rather, what is needed is excellent localization precision (i.e., the ability to determine the center of a single object). Localization precision always exceeds resolution. Indeed, localization precision of 1/10th of a pixel and 1/100th of the resolution limit is common in optical microscopy.[24,25] AFM images are a convolution of tip and sample geometry. Thus, to demonstrate tip−sample stability, we will track the center of an object through a series of successive images.

Such image-based verification of stability and registration requires a stationary, unchanging object that can withstand over an hour of continuous imaging; apparent motion could arise from instability of the object relative to the coverslip[22] and from tip or sample degradation. To satisfy these requirements, we used single 5 nm diameter Au nanospheres, which are known to be robust and incompressible,[26] and imaged with silicon nitride tips at modest forces (∼200 pN). We acquired seven sequential images over 82 min. Images at the beginning, middle, and end of the time course are displayed in Figure 5a−c.

To track the nanosphere's location with subpixel precision, we determined its center point using a 2D cross-correlation.[24,27] Specifically, we used the first image (Figure 5a) as the kernel to analyze the subsequent six images. Each cross-correlation yielded a Gaussian-like peak (Figure 5d). We fit the central 5 nm of the cross-correlation to a 2D Gaussian and localized the peak with excellent precision [<10 pm (1/50th pixel)] in each axis due in part to the high *S/N* of the images. As an example (Figure 5e), we plot a 1D slice centered vertically on the 2D cross-correlation peak (Figure 5d, black dotted line) with both the cross-correlation (dots) and the corresponding slice of the Gaussian fit (red line). From this analysis, we deduced the nanosphere's location [e.g., $x_p = 25.199 \pm 0.004$ nm (peak $\pm \sigma_{fit}$)], which is indicated graphically in Figure 5e (dashed line, line thickness $= 5\ \sigma_{fit}$).

This precise cross-correlation analysis tracked the nanosphere's location during 82 min of continuous imaging (Figure 5f). The precision of this control (and analysis technique) is further verified by small average deviations (23 and 40 pm in x and y, respectively) of the nanosphere's location from the linear fits. The residual lateral drift rates were a mere 4 and 5 pm/min in x and y, representing a 250-fold reduction of the inherent instrumental drift rate (Supporting Information, Figure S1) and a 100-fold improvement over current state of the art.[14] Indeed, these residual rates, achieved in air at room temperature, are close to those found in cryogenic conditions (∼1 pm/min, 8 K).[28] Further, these rates represent an upper bound for the actual drift since the analysis assumes a stationary object and no degradation of the tip or sample.

In this work, we utilized transparent substrates. Since the detection beams pass through the sample, the current instrument is not compatible with bulk metal and opaque

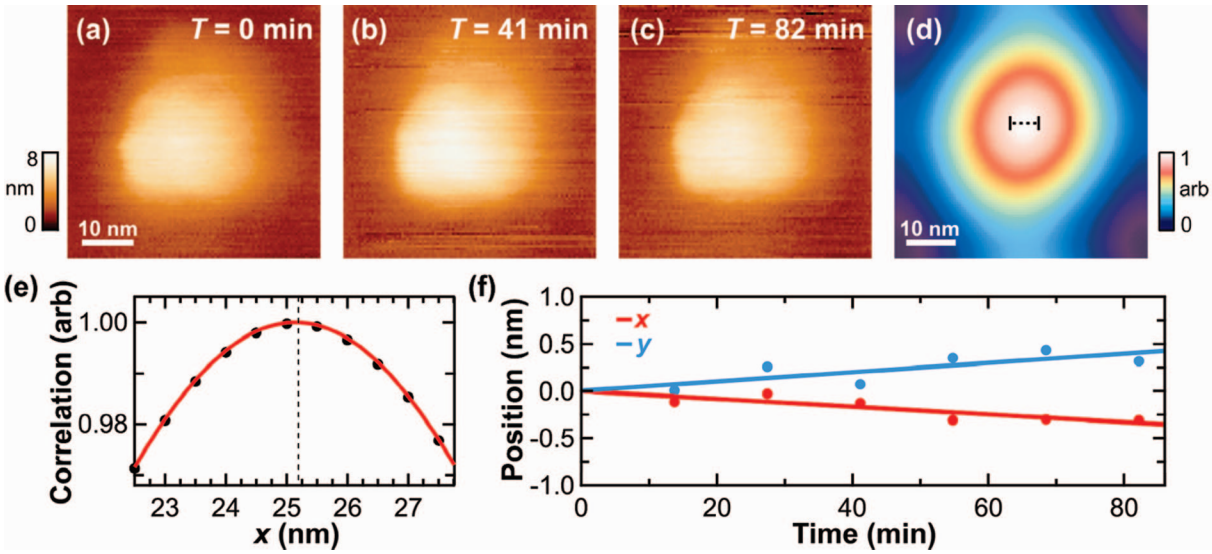

Figure 5. Ultrastable AFM imaging and residual drift analysis. (a−c) Images of a 5 nm gold nanosphere taken at times $T = 0$, 41, and 82 min, respectively. (d) The 2D cross-correlation between the first and last images. (e) A 1D slice (dots) through the 2D cross-correlation is plotted with the corresponding Gaussian fit (red line). The nanosphere's location [$x_p = 25.199 \pm 0.004$ nm (peak $\pm$ σ_{fit})] is indicated graphically (dashed line thickness $= 5\sigma_{fit}$). This 1D slice is centered vertically on the 2D cross-correlation peak (black dotted line in panel d). (f) Relative lateral position of the nanosphere plotted vs time as determined by cross-correlation analysis [x (red), y (blue)]. From linear fits to the data (lines), we deduced residual lateral drift rates of 4 and 5 pm/min in x and y, respectively.

samples. We anticipate that this technique could be generalized to a broader range of substrates and imaging conditions (see Supporting Information, Figure S2). For example, silicon wafers, in lieu of cover glass, can be accommodated by shifting to longer wavelength lasers where silicon is transparent. Alternatively, a fiducial mark could be engineered into the cantilever that spatially separates the tip from its fiducial mark, analogous to the silicon disk currently used to deduce sample motion. Such separation would enable strongly scattering or optically opaque samples to be studied with a similar degree of stability and registration.

To date, achieving atomic-scale tip−sample stability and registration require operating in a few highly specialized environments (ultrahigh vacuum[12] or cryogenic temperatures[28]), neither of which are conducive to biological studies or nanomanufacturing. Here, we have shown that scattering laser light off the apex of commercial AFM tips provides a robust means to an ultrastable AFM in ambient conditions. This approach should be compatible with dynamic cantilever detection methods; the high-frequency, low-amplitude tip oscillations will rapidly average to a mean tip position. In addition to imaging, control of the tip in 3D while it is disengaged from the surface should significantly enhance dynamic force spectroscopy.[2,29] For instance, stabilized F versus z curves will be especially useful in long time-scale studies such as protein refolding investigations.[30,31] Thus, we anticipate that this ultrastable AFM technology will find applications ranging from tip-based nanomanufacturing to fundamental studies in single-molecule biophysics.

Acknowledgment. The authors thank Alan Pattee and Hans Green for custom machining and design as well as Daniel Branton, Jene Golovchenko, and Christopher Russo for discussions. We also thank Charles Asbury, Matthew Côté, Scott Jordan, and Joshua Shaevitz for software and related assistance. This work was supported by a Burroughs Wellcome Fund Career Award at the Scientific Interface (G.M.K.), a National Research Council Research Associateship (G.M.K.), an Optical Science and Engineering Program NSF-IGERT Grant (A.R.C.), a National Physical Science Consortium Fellowship (A.R.C.), a PI NanoInnovation grant (A.R.C.), an NIH Molecular Biophysics Training Scholarship (A.B.C., T32 GM-065103), a Burroughs Wellcome Fund Career Award in the Biomedical Sciences (T.T.P.), a Butcher Grant (T.T.P.), the National Science Foundation (Phy-0404286 and Phy-1551010), and NIST. Mention of commercial products is for information only; it does not imply NIST's recommendation or endorsement. T.T.P. is a staff member of NIST's Quantum Physics Division.

Supporting Information Available: Detailed description of sample preparation protocol, laser alignment and calibration method, and stabilized imaging technique. Further, we show time-varying drift rates require high-bandwidth control (Figure S1), backscattered tip signals from AFM tips in air and water through different substrates (Figure S2), and highly linear and orthogonal stabilized scanning (Figure S3). This material is available free of charge via the Internet at http://pubs.acs.org.

References

(1) Giessibl, F. J. *Rev. Mod. Phys.* **2003**, *75*, 949–983.
(2) Müller, D. J.; Sapra, K. T.; Scheuring, S.; Kedrov, A.; Frederix, P. L.; Fotiadis, D.; Engel, A. *Curr. Opin. Struct. Biol.* **2006**, *16*, 489–495.
(3) Piner, R. D.; Zhu, J.; Xu, F.; Hong, S.; Mirkin, C. A. *Science* **1999**, *283*, 661–663.
(4) Dai, H. J.; Hafner, J. H.; Rinzler, A. G.; Colbert, D. T.; Smalley, R. E. *Nature* **1996**, *384*, 147–150.
(5) Li, M.; Tang, H. X.; Roukes, M. L. *Nat. Nanotechnol.* **2007**, *2*, 114–120.
(6) Viani, M. B.; Schaffer, T. E.; Chand, A.; Rief, M.; Gaub, H. E.; Hansma, P. K. *J. Appl. Phys.* **1999**, *86*, 2258–2262.
(7) Schimmel, T.; Koch, T.; Kuppers, J.; Lux-Steiner, M. *Appl. Phys. A* **1999**, *68*, 399–402.

(8) Ohnesorge, F.; Binnig, G. *Science* **1993**, *260*, 1451–1456.
(9) Radmacher, M.; Fritz, M.; Hansma, H. G.; Hansma, P. K. *Science* **1994**, *265*, 1577–1579.
(10) Pohl, D. W.; Moller, R. *Rev. Sci. Instrum.* **1988**, *59*, 840–842.
(11) Thomson, N. H.; Fritz, M.; Radmacher, M.; Cleveland, J. P.; Schmidt, C. F.; Hansma, P. K. *Biophys. J.* **1996**, *70*, 2421–2431.
(12) Abe, M.; Sugimoto, Y.; Namikawa, T.; Morita, K.; Oyabu, N.; Morita, S. *Appl. Phys. Lett.* **2007**, *90*, 203103.
(13) Horcas, I.; Fernandez, R.; Gomez-Rodriguez, J. M.; Colchero, J.; Gomez-Herrero, J.; Baro, A. M. *Rev. Sci. Instrum.* **2007**, *78*, 013705.
(14) Mokaberi, B.; Requicha, A. A. G. *IEEE T. Autom. Sci. Eng.* **2006**, *3*, 199–207.
(15) Proksch, R.; Dahlberg, E. D. *J. Appl. Phys.* **1993**, *73*, 5808–5810.
(16) Sparks, A. W.; Manalis, S. R. *Appl. Phys. Lett.* **2004**, *85*, 3929–3931.
(17) Teague, E. C. *J. Vac. Sci. Technol. B* **1989**, *7*, 1898–1902.
(18) Moon, E. E.; Smith, H. I. *J. Vac. Sci. Technol. B* **2006**, *24*, 3083–3087.
(19) Moon, E. E.; Kupec, J.; Mondol, M. K.; Smith, H. I.; Berggren, K. K. *J. Vac. Sci. Technol., B* **2007**, *25*, 2284–2287.
(20) Denk, W.; Webb, W. W. *Appl. Opt.* **1990**, *29*, 2382–2391.
(21) Carter, A. R.; King, G. M.; Perkins, T. T. *Opt. Express* **2007**, *15*, 13434–13445.
(22) Carter, A. R.; King, G. M.; Ulrich, T. A.; Halsey, W.; Alchenberger, D.; Perkins, T. T. *Appl. Opt.* **2007**, *46*, 421–427.
(23) Meyer, G.; Amer, N. M. *Appl. Phys. Lett.* **1988**, *53*, 1045–1047.
(24) Gelles, J.; Schnapp, B. J.; Sheetz, M. P. *Nature* **1988**, *331*, 450–453.
(25) Yildiz, A.; Forkey, J. N.; McKinney, S. A.; Ha, T.; Goldman, Y. E.; Selvin, P. R. *Science* **2003**, *300*, 2061–2065.
(26) Vesenka, J.; Manne, S.; Giberson, R.; Marsh, T.; Henderson, E. *Biophys. J.* **1993**, *65*, 992–997.
(27) Pratt, W. K. *Digital Image Processing*, 4th ed.; John Wiley & Sons: Hoboken, NJ, 2007.
(28) Stipe, B. C.; Rezaei, M. A.; Ho, W. *Science* **1998**, *280*, 1732–1735.
(29) Rief, M.; Gautel, M.; Oesterhelt, F.; Fernandez, J. M.; Gaub, H. E. *Science* **1997**, *276*, 1109–1112.
(30) Carrión-Vázquez, M.; Oberhauser, A. F.; Fowler, S. B.; Marszalek, P. E.; Broedel, S. E.; Clarke, J.; Fernandez, J. M. *Proc. Natl. Acad. Sci. U.S.A.* **1999**, *96*, 3694–3699.
(31) Kessler, M.; Gottschalk, K. E.; Janovjak, H.; Müller, D. J.; Gaub, H. E. *J. Mol. Biol.* **2006**, *357*, 644–654.

NL803298Q